



# Comparison of the Catalytic Activity of Carbon, Spinel-Based, and Carbide Materials in the Na-Air Battery

Evelina Faktorovich-Simon<sup>1</sup>, Amir Natan<sup>2</sup>, Emanuel Peled<sup>1\*</sup> and Diana Golodnitsky<sup>1,3\*</sup>

<sup>1</sup> School of Chemistry, Tel Aviv University, Tel Aviv, Israel, <sup>2</sup> Department of Physical Electronics, Tel Aviv University, Tel Aviv, Israel, <sup>3</sup> Wolfson Applied Materials Research Center, Tel Aviv University, Tel Aviv, Israel

## OPEN ACCESS

### Edited by:

Piercarlo Mustarelli,  
University of Milano Bicocca, Italy

### Reviewed by:

Vito Di Noto,  
University of Padova, Italy  
Bao Yu Xia,  
Huazhong University of Science and  
Technology, China

### \*Correspondence:

Emanuel Peled  
peled@tauex.tau.ac.il  
Diana Golodnitsky  
golod@tauex.tau.ac.il

### Specialty section:

This article was submitted to  
Energy Materials,  
a section of the journal  
Frontiers in Materials

Received: 11 July 2019

Accepted: 19 September 2019

Published: 04 October 2019

### Citation:

Faktorovich-Simon E, Natan A,  
Peled E and Golodnitsky D (2019)  
Comparison of the Catalytic Activity of  
Carbon, Spinel-Based, and Carbide  
Materials in the Na-Air Battery.  
Front. Mater. 6:249.  
doi: 10.3389/fmats.2019.00249

Rechargeable sodium-oxygen batteries have attracted much interest in recent years, owing to their high theoretical specific energy, and the abundance of sodium. The material of which the cathode is constructed influences the performance of the battery. In this study, we show that low-surface-area glassy carbon (GC) cannot operate for more than four consecutive cycles, whereas high-surface-area carbon materials, such as Black Pearl 2000 carbon (BP 2000), significantly increase the number of cyclic-voltammetry runs, without current reduction. NiCo<sub>2</sub>O<sub>4</sub> was previously considered a promising material for the cathode. However, its activity was not compared with the only carbon-based electrode. Here we compare the electrochemical performance of four different Ni<sub>x</sub>Co<sub>y</sub>O<sub>z</sub> powders to BP 2000, XC72R, and SB carbon. The highest activity was obtained with the use of a powder, which contained 45% NiCo<sub>2</sub>O<sub>4</sub>, 10% CoO, 30% metallic nickel, and 15% metallic cobalt. We believe that the metallic nickel and cobalt phases are responsible for this high catalytic activity. Accelerated stress tests of XC72R, BP 2000, SB, and TiC powders, after 100 cyclic-voltammetry cycles, revealed that TiC exhibited the greatest loss of reduction peak area (~57%) during the test, indicating the highest loss of catalytic activity. It also exhibited higher loss of oxidation peak area than Vulcan XC72R (~68% vs. ~35%), but lower than BP 2000 (~90%) and SB carbon (~72%). The reason for such a high degradation probably comes from strong surface changes or loss of adhesion of the catalyst powder to the GC electrode during the AST. It was suggested that in most cases, it is the OER process, which exhibits stronger deterioration.

**Keywords:** sodium-air batteries, oxygen redox processes, PEGDME, catalyst, cyclic voltammetry

## INTRODUCTION

Rechargeable sodium-oxygen batteries have attracted much interest in recent years, thanks to their high theoretical specific energy, lower charge overpotential than lithium-oxygen batteries and the abundance of sodium. The first molten-sodium-oxygen cell was constructed in Peled's group in 2011. It was shown that this cell can be cycled several times (Peled et al., 2011). Another advantage of the Na-air system is that, in contrast to lithium, sodium does not dissolve in aluminum (0.003%) and this enables the use of aluminum as a light and low-cost hardware material, especially for thin bipolar plates. While in lithium-oxygen batteries, Li<sub>2</sub>O<sub>2</sub> was identified as the sole discharge

product, in sodium-oxygen batteries, at least three different discharge products have been reported: sodium superoxide, peroxide dihydrate, and dehydrated sodium peroxide ( $\text{NaO}_2$ ,  $\text{Na}_2\text{O}_2 \cdot 2\text{H}_2\text{O}$ , and  $\text{Na}_2\text{O}_2$ ) (Hartmann et al., 2014; Kwak et al., 2015; Pinedo et al., 2016).  $\text{NaO}_2$ -based batteries show low overpotentials and high coulombic efficiencies, while in  $\text{Na}_2\text{O}_2$ -based batteries, notably higher overpotentials are reported (Hartmann et al., 2013; Kim et al., 2016; Pinedo et al., 2016). Consequently,  $\text{NaO}_2$  cells show better cycleability than their  $\text{Na}_2\text{O}_2$  analogs. Parameters which determine the type of the discharge products could be, for example, the solvent mixture, the type of conducting salt, oxygen purity, applied current density, and the material of the positive electrode (air electrode).

Bender et al. studied the influence of several types of carbon materials on the stoichiometry of the discharge products, and on cell performance (Bender et al., 2014). They found that, for all types of carbon studied, phase-pure  $\text{NaO}_2$  is always found as a discharge product. However, it had a strong influence on the discharge capacity of the battery. Their additional study on carbon-nanotube-based electrodes also supported these findings (Bender et al., 2015). Antonio Elia et al. also found  $\text{NaO}_2$  as the major discharge product in the battery with the air electrode comprising multi-walled carbon nanotubes, coated on a gas-diffusion layer (Elia et al., 2016). However, in several studies,  $\text{Na}_2\text{O}_2$  was found as the discharge product (Li et al., 2013; Liu et al., 2013). For example, Sun et al. and Yadegari et al. found independently that a mixture of  $\text{Na}_2\text{O}_2$  and  $\text{NaO}_2$  was generated as the discharge product, when an air electrode was composed of nitrogen-doped carbon nanotubes, under dry-air conditions (Yadegari et al., 2014, 2015; Sun et al., 2015). Ma et al. conducted a study on co-embedded N-doped carbon fibers as the air electrode, and found poor crystallinity  $\text{Na}_2\text{O}_2$  as the main discharge product in their cells (Ma et al., 2017). Liu et al. also found dependence of the morphology of the discharge products on the material and structure of the air electrode. They established that hierarchically macroporous framework in the rGO (reduced graphene oxide) electrode allows dense and continuous growth of the cubic discharge products, in sodium-oxygen cells. The grain sizes of these products are larger than those which grow in a mesoporous electrode, and cause less pore clogging (Liu et al., 2016; Schröder et al., 2016). Up to now, only a few studies have been made on the metal-oxide-based air electrodes. High discharge capacity found in the research of Shang et al. has been linked to the composition and shape of the catalyst particles ( $\text{MnCo}_2\text{O}_4$  microspheres) on a carbon-supported composite air electrode. However, strong capacity fading was observed under full discharge and charge conditions (Shang et al., 2017). To the best of our knowledge, the only study on the non-carbon-supported air electrode, for sodium-oxygen batteries, was made on  $\text{NiCo}_2\text{O}_4$  nanosheets supported by Ni foam (Liu et al., 2014). In this study,  $\text{Na}_2\text{O}_2$  nanosheets were observed as the discharge product, and it was concluded that the electrocatalytic activity of  $\text{NiCo}_2\text{O}_4$  nanosheets/Ni are promising for the air electrode in rechargeable sodium-air batteries. However,  $\text{NiCo}_2\text{O}_4$  activity was not compared with that of the carbon-only-based electrode.

Our study focused on the comparison of the electrocatalytic activity of several commercial carbons, homemade  $\text{Ni}_x\text{Co}_y\text{O}_z$  compounds and TiC powders.

$\text{NiCo}_2\text{O}_4$  is a spinel-type oxide, which comprises a mixture of NiO and  $\text{Co}_3\text{O}_4$ . Therefore, the resultant mixed oxide may contain separate NiO and  $\text{Co}_3\text{O}_4$  phases. It was found that the NiO phase lowers the catalytic activity of  $\text{NiCo}_2\text{O}_4$ , in alkaline media (Tseung and Jasem, 1977). In our study, we determined the catalytic activity of different phase structures of the homemade  $\text{Ni}_x\text{Co}_y\text{O}_z$  powders.

Transition metal carbides (TMCs) have been extensively studied as cathode materials in Li- $\text{O}_2$  batteries, because of their high electrical conductivity and chemical stability. TiC was previously considered a promising material for the air electrode in lithium-oxygen batteries. Thotiyl et al. compared the electrode performance of the TiC-based air electrode with that of the carbon-based air electrode, for lithium-oxygen batteries (Ottakam Thotiyl et al., 2013). They found that the TiC-based air electrode greatly reduced side reactions as compared to carbon, and concluded that TiC appears to be a more viable and stable air-electrode material. Adams et al. studied the influence of insulating  $\text{TiO}_2$  layers on the TiC surface, on its activity for the oxygen-evolution reaction, for lithium-oxygen batteries. The authors state that these layers, even as thin as 3 nm, can completely inhibit its oxygen-evolution activity (Adams et al., 2014). Raz et al. have performed a theoretical analysis of the adsorption of  $\text{Li}_2\text{O}_2$ ,  $\text{NaO}_2$ , and  $\text{Na}_2\text{O}_2$  on the pristine and oxidized TiC(111) surface (Raz et al., 2018). However, TiC activity and durability has not yet been studied for sodium-oxygen batteries. In our study, we have estimated, for the first time, TiC electrocatalytic activity for sodium-oxygen batteries. In addition, we have compared TiC activity with the activity of several commercial types of carbon. We have also evaluated the durability of TiC electrode by estimating its catalytic properties after 100 ORR/OER cycles.

## MATERIALS AND METHODS

Cyclic voltammetry and RDE experiments were carried out in a portable airtight glove bag purged with dry argon or oxygen, at room temperature, with the use of AUTOLAB potentiostat PGSTAT302N. The measurements were performed in the glass cell with three-electrode configuration, utilizing RRDE-3A Apparatus (ALS, Japan). Before each experiment, the working glassy carbon (GC) disc electrode, with a diameter of 3 mm, was polished with  $0.05 \mu\text{m}$   $\text{Al}_2\text{O}_3$  suspension, on a moistened polishing Micro-Cloth (both from Buehler). Following this, the electrode was dried for 5 h in a vacuum chamber, at room temperature. A platinum coil was used as the counter electrode. The reference electrode was a commercial non aqueous  $\text{Ag}/\text{Ag}^+$  electrode. The reference-electrode potential was checked vs. sodium, and was reported vs. the  $\text{Na}/\text{Na}^+$  couple. Dry oxygen (99.999%) was bubbled through the electrolyte solution for 60 min prior to the ORR experiments. Moisture and hydrocarbon traps (M. SNIR technological services Ltd.)

were installed in the oxygen tubing, before placing the cell in the airtight glove bag. All the experiments were carried out at room temperature. The current densities of the ORR and OER were normalized for the BET surface area of the powders.

PEGDME 500 (Merck KGaA) was dried three times over activated molecular sieves (4 Å type). Each time, the pre-used molecular sieves were removed from PEGDME 500 after 24 h of drying, and new molecular sieves were introduced to the solvent for another 24 h. NaOTf (99.5%, SOLVOIONIC) was dried in the vacuum oven at 100°C, for 5 h. TiC nanopowder (<200 nm, Sigma-Aldrich), and Black pearls 2000, Shawinigan Black, XC72R carbon powders were dried under vacuum for 5 h at 100°C.

The process of synthesis of  $Ni_xCo_yO_z$  powders was as follows. 0.4 M HCl +  $NiCl_2$  solution was mixed with 0.4 M HCl +  $CoCl_2$  solution, and stirred for 1 h. The amount of  $NiCl_2$  and  $CoCl_2$  powders in the HCl solutions was according to the desired Ni:Co ratio in the final powder. Thirty-two percent ammonium hydroxide solution was added to the mixed solution, until  $pH \approx 11$  was achieved. An excess of  $NaBH_4$  was dissolved in water, and added to the mixture of the salt solutions during stirring. The obtained suspension was centrifuged, and the sediment was separated from the solution. The sediment was washed repeatedly with distilled water until no chloride ions were detected. The  $Ni_xCo_yO_z$  powders obtained were dried by water evaporation at 100°C, and annealed at 300°C or at 445°C, for 12 h, in order to examine the effect of temperature on the crystallographic structure and catalytic activity of the powders. All the powders obtained were vacuum-dried at 100°C, for 5 h, prior to experiments.

The powders were analyzed with the use of a Scintag X-ray powder diffractometer with a Cu X-ray source, equipped with a liquid-nitrogen-cooled intrinsic Ge solid-state detector. SEM imaging and elemental analysis of the powders were obtained using a JOEL (JSM-6300) scanning-electron microscope (JSM-6300), with X-ray LINK detector and Pentafen window. XPS analysis of the TiC surface was carried out with a PHI 5600 Multi-Technique System with a base pressure of  $2.5 \times 10^{-10}$  Torr. The samples were irradiated by an Al  $K\alpha$  monochromatic source (1486.6 eV), and the scattered electrons were analyzed by a spherical capacitor analyzer, having a slit aperture of 0.8 mm.

BET measurements were conducted with the use of a NOVA 2200e analyzer (Quantachrome instruments). The samples were degassed under vacuum at temperature of 100°C, for 3 h prior to the analysis.

Catalyst ink was prepared by sonication of the catalyst powder suspension in a solution of PVP in cyclopentanone (10%wt PVP:90%wt catalyst powder), for 1 h. Two microliter of the ink was dropped on the glassy-carbon electrode, which was left in the argon-filled glovebox with water content <0.1 ppm, for cyclopentanone evaporation. The electrodes with the ink coating were dried for an additional 5 h in a vacuum chamber, at room temperature.

## RESULTS AND DISCUSSION

The electrocatalytic behavior of the oxygen-reduction reaction (ORR) and the oxygen-evolution reaction (OER) was examined first on the neat glassy-carbon (GC) electrode (**Figure 1**).

One reduction and one oxidation peak can be observed in the figure. It is known that the first reduction step is a one-electron reduction of  $O_2$ , in which, presumably,  $NaO_2$  forms (Equation 1) (Laoire et al., 2009).  $NaO_2$  is then oxidized, in the back scan to  $O_2$  and  $Na^+$ . It can be seen from the figure that reduction- and oxidation-peak currents on the neat GC electrode decrease with cycling. By the fourth scan, there was almost no current observed. Such behavior may indicate accumulation on the electrode of low-conductivity or insulating reduction products, such as  $Na_2O_2$ .  $Na_2O_2$  probably forms as a result of chemical disproportionation of  $NaO_2$  (Equation 2), and cannot

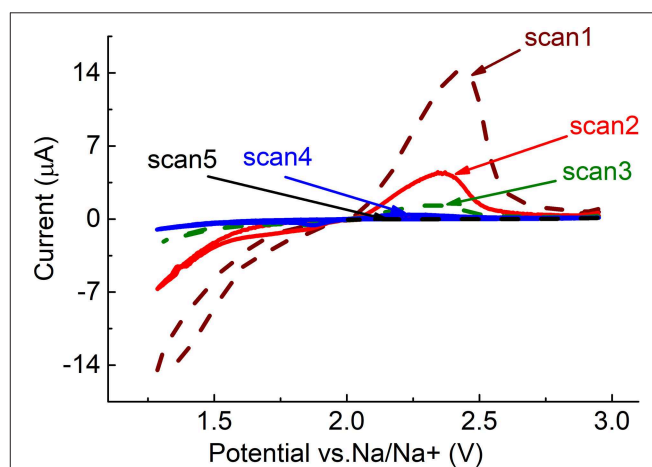


**FIGURE 1** | Five first cycles on GC electrode in PEGDME/0.25 M NaOTf (Scan rate 5 mV/s, at 1.25 to 3.0 V).

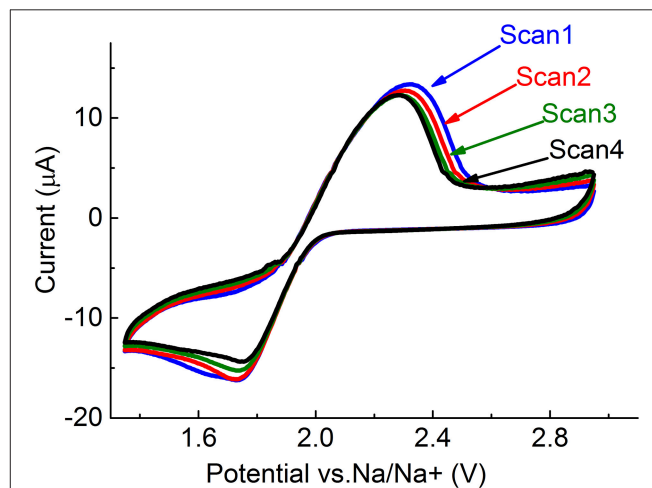


**FIGURE 2** | Five first cycles of BP 2000 coated on GC electrode in PEGDME/0.25 M NaOTf (Scan rate 5 mV/s) ( $40 \mu g/cm^2$ ).

be oxidized within the selected potential window. In order to oxidize  $\text{Na}_2\text{O}_2$ , the potential window must be extended to  $\sim 4.5$  V (Figure 6). However, extension of the potential window can cause oxidation of the electrolyte and the electrode material, as in the case of lithium-oxygen batteries, formation of undesirable byproducts, and reduced cycleability of the cell (Ottakam Thotiyil et al., 2013). In order to avoid extension of the potential window, but to enable effective operation of the cell, high-surface-area electrode materials can be used. These materials can accommodate much more low-conductivity discharge products, and still provide electrical contact for the current flow. The electrochemical performance of Black Pearls carbon (BP 2000), coated on the GC electrode, confirm this. Figure 2 shows that on cycling, the current peak decreases to a much lesser degree on the electrode coated with Black pearls 2000, than on the neat GC.



As previously mentioned,  $\text{NiCo}_2\text{O}_4$  was proposed as a promising material for rechargeable sodium-air batteries. Therefore, we compared its catalytic activity to that of BP 2000 carbon. In order to study the influence of nickel and cobalt content on the crystal structure and electrochemical performance of  $\text{Ni}_x\text{Co}_y\text{O}_z$  catalysts, powders with different ratios of nickel and cobalt were

synthesized. The powders were annealed and analyzed with the use of EDS, XRD, SEM, and BET techniques.

## EDS, XRD, SEM, and BET Tests of $\text{Ni}_x\text{Co}_y\text{O}_z$ Powders

EDS analysis showed that two  $\text{Ni}_x\text{Co}_y\text{O}_z$  powders with atomic Ni:Co ratios of 35:65, and 20:80 were obtained as a result of the synthesis. The first  $\text{Ni}_x\text{Co}_y\text{O}_z$  powder was annealed at  $445^\circ\text{C}$  for 12 h (Ni:Co\_35:65\_445°C). The second one was tested as obtained (Ni:Co\_20:80\_no annealing), and after annealing at two temperatures:  $300^\circ\text{C}$  (Ni:Co\_20:80\_300°C) and  $445^\circ\text{C}$  (Ni:Co\_20:80\_445°C). Elemental and crystallographic composition, annealing temperature, and BET surface area of the four obtained powders are summarized in Table 1.

Figure 3A presents the XRD pattern of  $\text{Ni}_x\text{Co}_y\text{O}_z$  powder with Ni:Co ratio of 20:80, before and after annealing at  $445^\circ\text{C}$ . Before annealing, there were no evident peaks observed, a fact which indicates the formation of an amorphous material. After annealing, several peaks appeared, which can be ascribed to the formation of  $\text{NiCo}_2\text{O}_4$ . However, XRD peaks of  $\text{NiCo}_2\text{O}_4$  and  $\text{Co}_3\text{O}_4$  are very close, and it is difficult to distinguish between them. The best fitting of the peaks was obtained for the composition of  $\text{NiCo}_2\text{O}_4$ —30%,  $\text{Co}_3\text{O}_4$ —60%, and 10% NiO (Figure 3B). A similar XRD pattern, except for the absence of

**TABLE 1** | Elemental and crystallographic composition, and BET of the synthesized  $\text{Ni}_x\text{Co}_y\text{O}_z$  powders.

Treatment	Ni:Co elemental composition	Annealing temperature (for 12 h)	Crystallographic phase	BET surface area ( $\text{m}^2/\text{g}$ )
Ni:Co_35:65_(445°C)	35:65	445°C	Ni—30% Co—15% CoO—10% $\text{NiCo}_2\text{O}_4$ —45%	9
Ni:Co_20:80_(no annealing)	20:80	No annealing	Amorphous NiCo	50
Ni:Co_20:80_(300°C)		300°C	$\text{NiCo}_2\text{O}_4$ —60% $\text{Co}_3\text{O}_4$ —40%	65
Ni:Co_20:80_(445°C)		445°C	$\text{NiCo}_2\text{O}_4$ —30% $\text{Co}_3\text{O}_4$ —60% NiO—10%	53

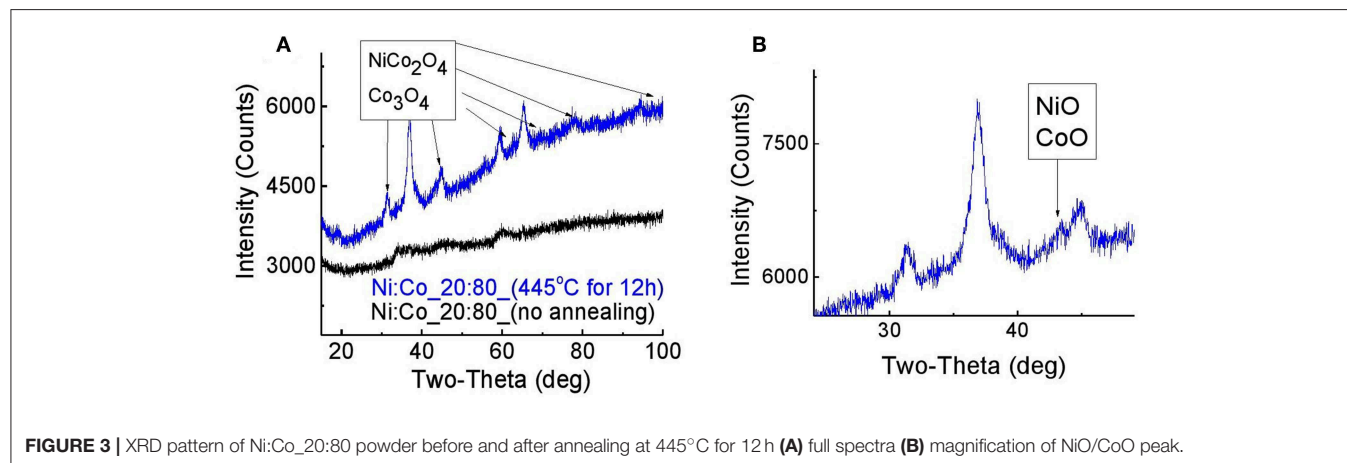


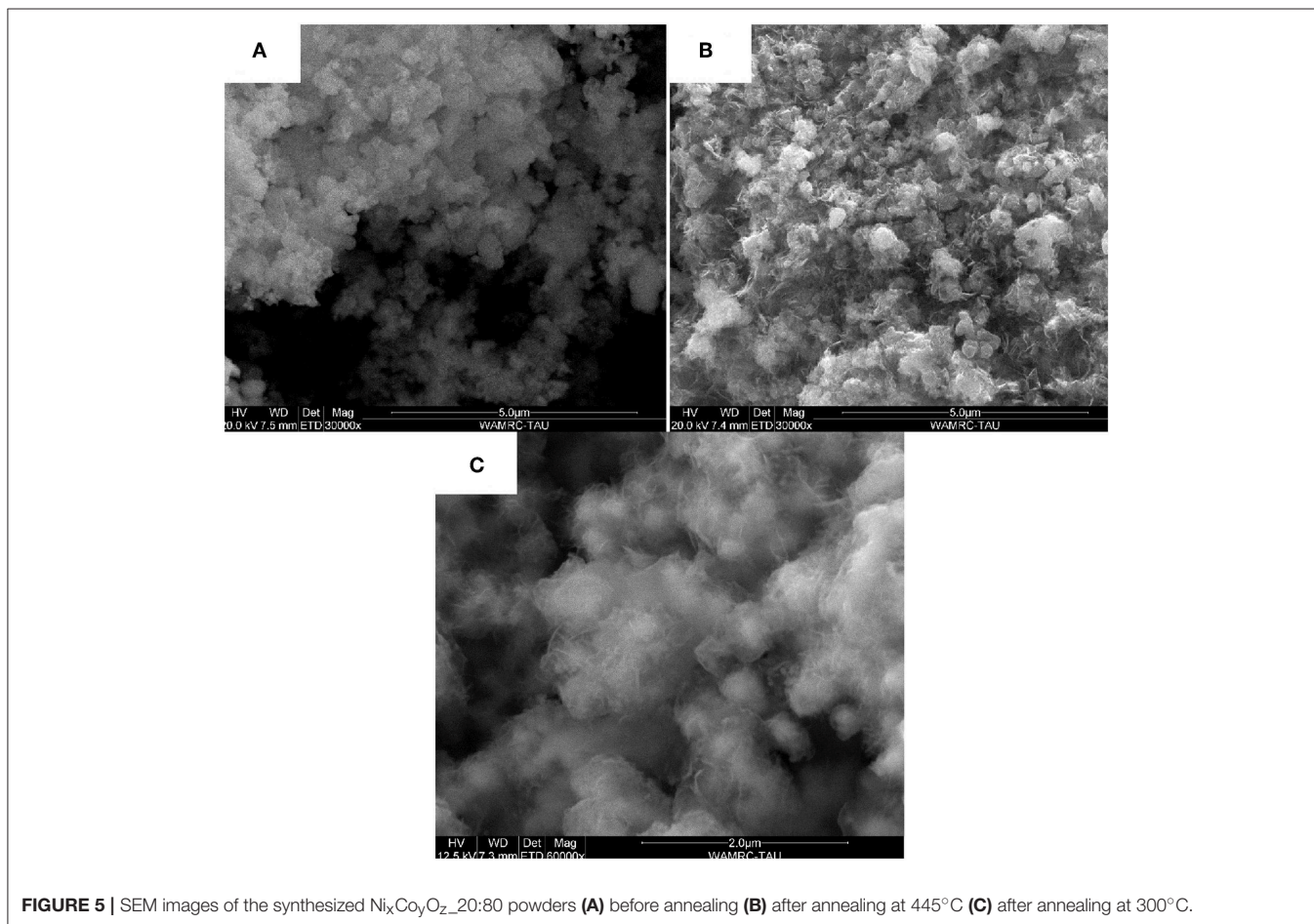
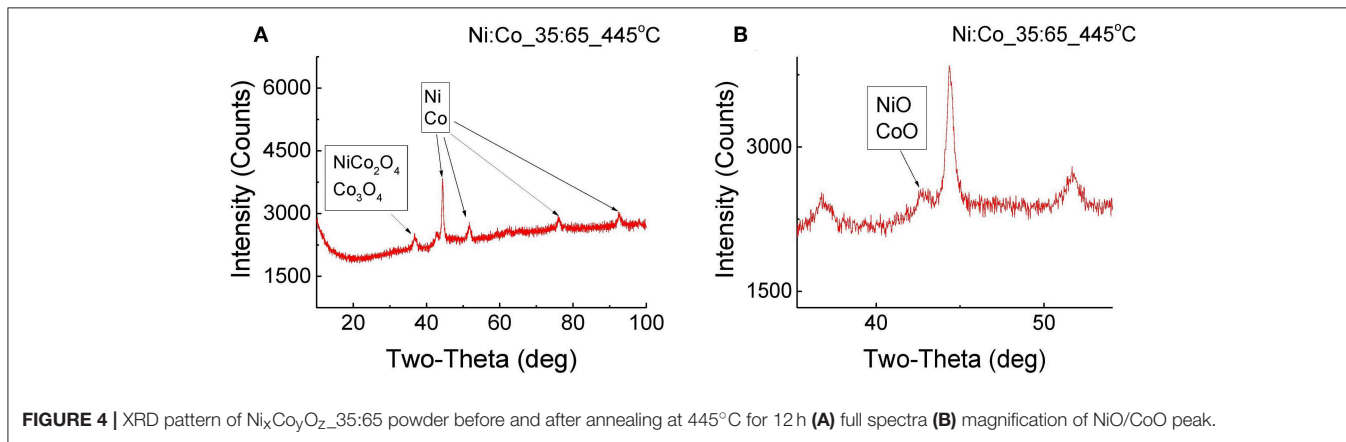
**FIGURE 3** | XRD pattern of Ni:Co\_20:80 powder before and after annealing at  $445^\circ\text{C}$  for 12 h (A) full spectra (B) magnification of NiO/CoO peak.

the NiO phase, was obtained for the same powder, which was annealed at 300°C.

A different XRD pattern was obtained for the powder with an Ni:Co ratio of 35:65, after annealing at 445°C. In **Figure 4A** we see peaks, which can be ascribed to metallic Ni or Co phases. Here also, Ni and Co XRD lines are very close to each other and it is difficult to distinguish between them. In addition, a small fraction of NiCo<sub>2</sub>O<sub>4</sub> or Co<sub>3</sub>O<sub>4</sub> phases can be observed. In **Figure 4B**, a

small peak, which can be related to NiO or CoO phases, can also be detected.

SEM images of the synthesized powders support the XRD results (see **Figure 5**). **Figure 5A** shows the morphology of the Ni<sub>x</sub>Co<sub>y</sub>O<sub>z</sub>\_20:80 powder before the annealing. The catalyst consists of spherical particles of about 100 nm in diameter. In the **Figures 5B,C**, after the annealing at 445°C and 300°C, respectively, thin plate-like entities can be seen in addition to



the spherical particles. These plates can indicate appearance of crystal  $\text{NiCo}_2\text{O}_4$  and  $\text{Co}_3\text{O}_4$  particles (Liu et al., 2014), which is consistent with the obtained XRD results. The same, plate-like structure was obtained for the  $\text{Ni}_x\text{Co}_y\text{O}_z$ \_35:65 powder, after the annealing.

## Electrochemical Performance of $\text{Ni}_x\text{Co}_y\text{O}_z$ Powders vs. BP 2000

Figures 6A,B show comparison between electrochemical performance of BP 2000, and of four synthesized  $\text{Ni}_x\text{Co}_y\text{O}_z$  powders coated on a GC electrode (about  $40 \mu\text{g}/\text{cm}^2$ ). Here, the reduction peak is ascribed to one-electron reduction of  $\text{O}_2$  to form  $\text{NaO}_2$ , for all the tested materials. Part of the  $\text{NaO}_2$  probably undergoes disproportionation to  $\text{Na}_2\text{O}_2$ , as in the case of glassy carbon. In the selected potential window, the oxidation peak is attributed to oxidation of  $\text{NaO}_2$  to  $\text{O}_2$  and  $\text{Na}^+$ . In order to oxidize  $\text{Na}_2\text{O}_2$ , the potential window should be extended to about 4.5 V, as at GC (see Figure 7). As previously mentioned (Hartmann et al., 2013; Kim et al., 2016; Pinedo et al., 2016),  $\text{NaO}_2$ -based sodium-oxygen batteries show lower overpotential, and higher coulombic efficiencies, as compared to the  $\text{Na}_2\text{O}_2$ -based ones. Higher fraction of  $\text{NaO}_2$ , produced during the reduction step, and ability of the catalyst to oxidize it, can indicate better catalytic activity of the material. The area of current density peaks can reflect the amount of produced (reduction area) and oxidized  $\text{NaO}_2$  (oxidation area). Table 2 summarizes the reduction and oxidation peak areas for all the examined powders. From the table we can see that reduction and oxidation areas of the powder with the highest  $\text{NiCo}_2\text{O}_4$  content (60%  $\text{NiCo}_2\text{O}_4$  and 40%  $\text{Co}_3\text{O}_4$ ) are the smallest, among the  $\text{Ni}_x\text{Co}_y\text{O}_z$  powders, which indicate the lowest catalytic activity toward generation and oxidation of  $\text{NaO}_2$ . The powder with 30%  $\text{NiCo}_2\text{O}_4$  and 60%  $\text{Co}_3\text{O}_4$  showed better electrochemical performance than the powder with 60%  $\text{NiCo}_2\text{O}_4$  and 40%  $\text{Co}_3\text{O}_4$ , despite the presence of the non-catalytic  $\text{NiO}$  phase in it. This suggests that  $\text{Co}_3\text{O}_4$  is more catalytic than  $\text{NiCo}_2\text{O}_4$  for ORR and OER, in sodium-oxygen cells. The highest activity was obtained using a powder, which contained 45%  $\text{NiCo}_2\text{O}_4$ , 10%  $\text{CoO}$ , 30% metallic nickel, and 15% metallic cobalt. It is known that not free-of-oxides metallic surfaces are more reactive

than the oxidized ones (Raz et al., 2018). Therefore, we believe that metallic nickel and cobalt phases are responsible for this high catalytic activity. However, additional studies should be conducted in order to evaluate quantitative contribution of these metallic phases to the catalytic properties of the powders. All the synthesized  $\text{Ni}_x\text{Co}_y\text{O}_z$  powders showed better activity than BP 2000. Molecular dynamic simulation studies of adsorption energies of oxygen and  $\text{NaO}_2$  molecules on the surface of the catalyst components could be helpful for the explanation of the findings mentioned above. Such work is planned to be done.

As in the case of the GC electrode, the oxidation peak of  $\text{Na}_2\text{O}_2$  also appeared in the CV acquired at a voltage window expanded to 4.5 V on  $\text{Ni}_x\text{Co}_y\text{O}_z$  catalyst (Figure 7). The area of  $\text{Na}_2\text{O}_2$  oxidation peak is 1.5 times higher than that of  $\text{NaO}_2$  (430 and  $280 \mu\text{C}/\text{cm}^2$ , respectively), in contrast to what was obtained with neat GC, where the  $\text{NaO}_2$  oxidation peak was twice ( $1040 \mu\text{C}/\text{cm}^2$ ) that the oxidation peak of  $\text{Na}_2\text{O}_2$  ( $450 \mu\text{C}/\text{cm}^2$ ). Lower oxidation peak of  $\text{NaO}_2$  indicates its smaller amount on the electrode, which can point toward facilitation of

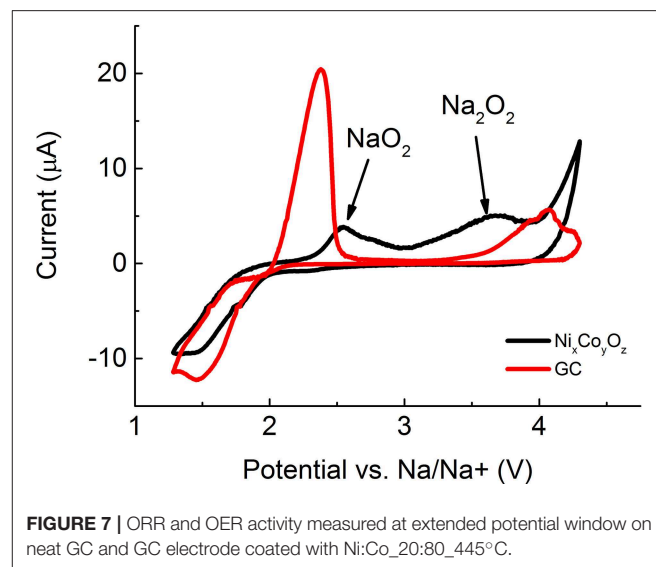


FIGURE 7 | ORR and OER activity measured at extended potential window on neat GC and GC electrode coated with  $\text{Ni}_x\text{Co}_y\text{O}_z$ .

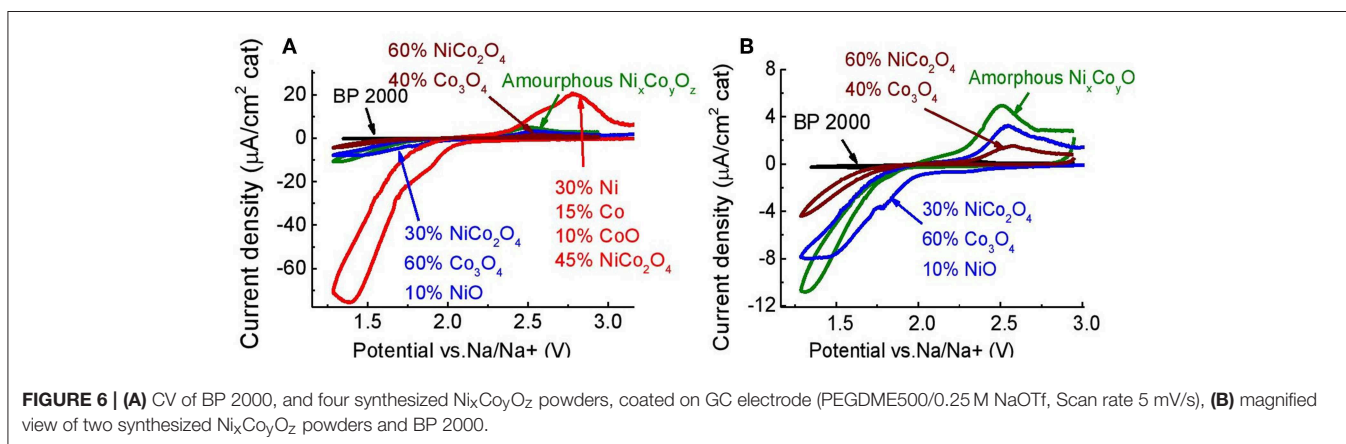


FIGURE 6 | (A) CV of BP 2000, and four synthesized  $\text{Ni}_x\text{Co}_y\text{O}_z$  powders, coated on GC electrode (PEGDME500/0.25 M  $\text{NaOTf}$ , Scan rate 5 mV/s), (B) magnified view of two synthesized  $\text{Ni}_x\text{Co}_y\text{O}_z$  powders and BP 2000.

chemical disproportionation of  $\text{NaO}_2$  to  $\text{Na}_2\text{O}_2$  on the surface of  $\text{Ni}_x\text{Co}_y\text{O}_z$  catalyst.

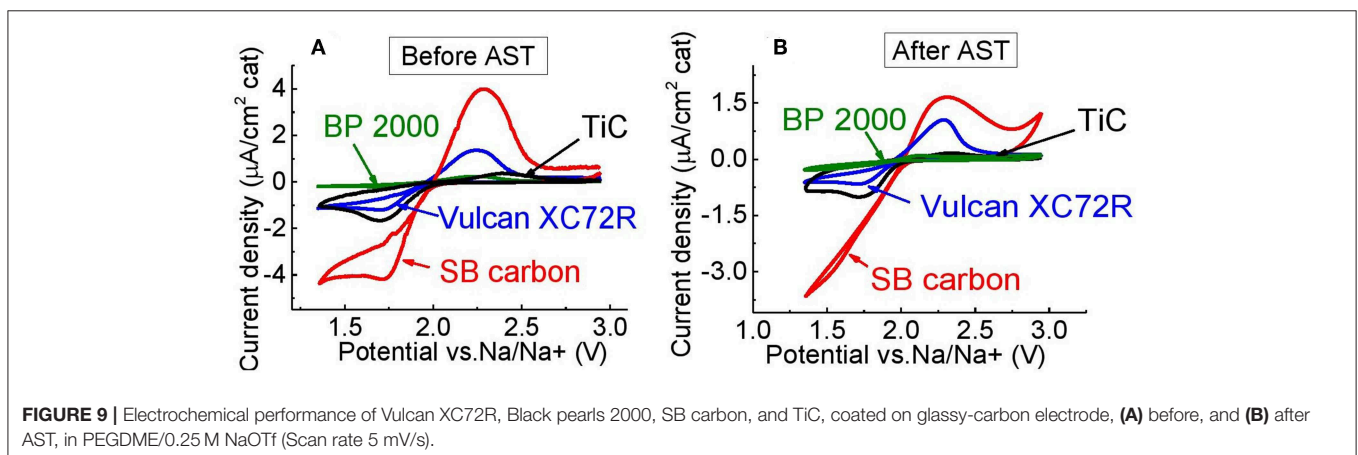
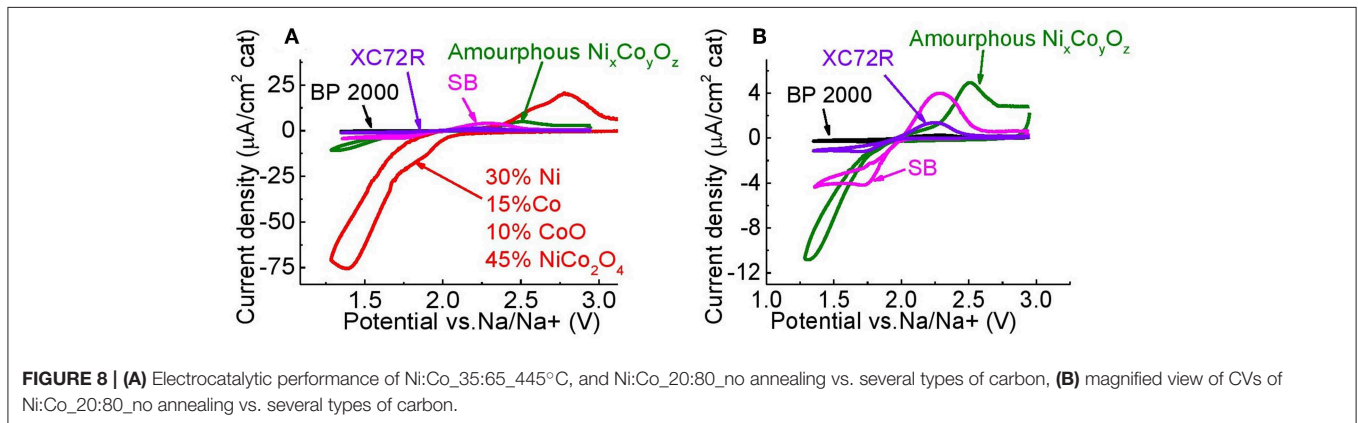
**Figures 8A,B** demonstrate ORR and OER current densities on a GC electrode coated with annealed Ni:Co\_35:65\_445°C and as-prepared Ni:Co\_20:80 catalysts, BP 2000, XC72R, and SB carbon. Loading of the catalysts on the GC was about 40  $\mu\text{g}/\text{cm}^2$ . Separation of ORR and OER current density peaks is larger in the case of  $\text{Ni}_x\text{Co}_y\text{O}_z$  powders (see **Table 2**), which can be ascribed to higher electrical resistance of the powders, as compared to the carbon materials. Despite this, the highest

current density peaks of ORR and OER were obtained for the annealed Ni:Co\_35:65 catalyst. The area of the reduction and oxidation peaks reflects the amount of  $\text{NaO}_2$ , which is generated and oxidized, respectively. From **Table 2** it appears that as-prepared Ni:Co\_20:80 coating also produces larger amount of  $\text{NaO}_2$  (larger areas of reduction and oxidation peaks) than do all the tested types of the commercial carbon, indicating enhanced ORR/OER performance of catalysts.

The electrochemical performances of XC72R, BP 2000, and SB carbon were compared to the performance of TiC powder,

**TABLE 2** | Summary of reduction and oxidation areas for the examined powders, and separation of ORR and OER peaks.

Powder	Reduction area	Oxidation area	Potential of ORR peak	Potential of OER peak	Peak separation
	$\mu\text{C}/\text{cm}^2$	$\mu\text{C}/\text{cm}^2$	V	V	V
$\text{Ni}_x\text{Co}_y\text{O}_z_{35:65}_{(445^\circ\text{C})}$	9,152	1,547	1.38	2.78	1.4
$\text{Ni}_x\text{Co}_y\text{O}_z_{20:80}_{(\text{no annealing})}$	1,094	463	1.31	2.51	1.2
$\text{Ni}_x\text{Co}_y\text{O}_z_{20:80}_{(300^\circ\text{C})}$	430	139	1.28	2.57	1.29
$\text{Ni}_x\text{Co}_y\text{O}_z_{20:80}_{(445^\circ\text{C})}$	1,184	289	1.44	2.55	1.11
BP 2000	44	15	1.74	2.28	0.54
XC72R	202	71	1.7	2.24	0.54
SB	752	261	1.71	2.28	0.57
TiC	187	32	1.7	2.4	0.7



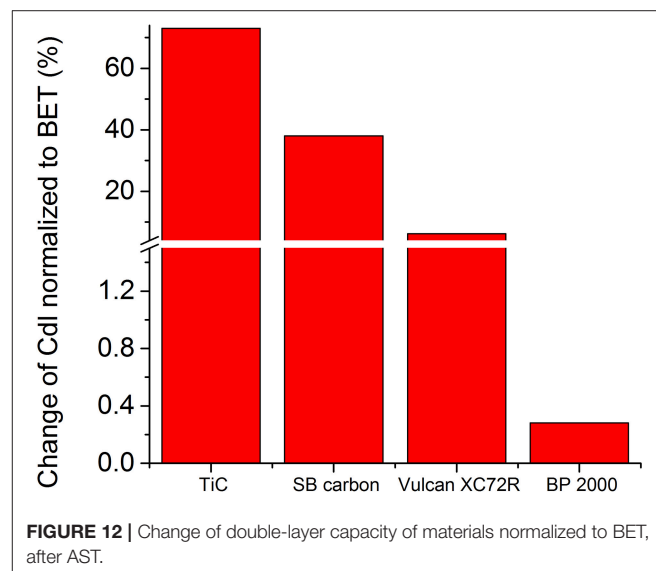
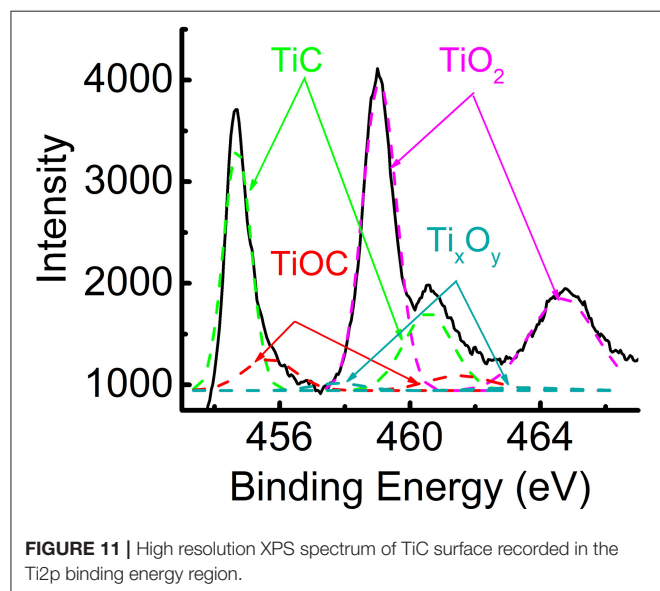
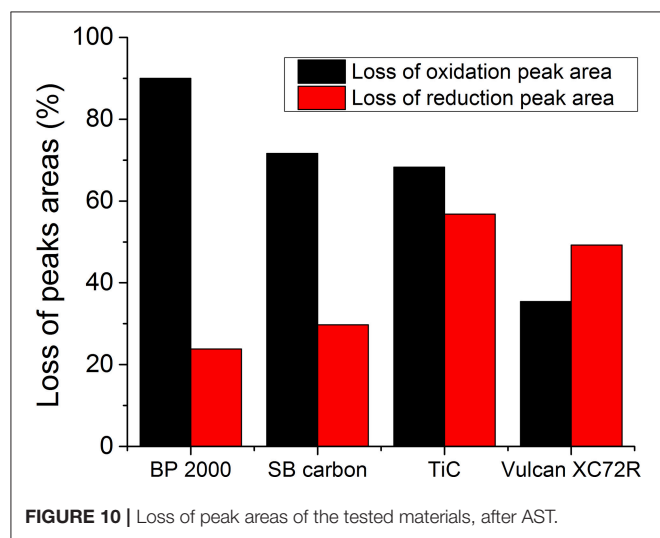
before and after an accelerated stress test (AST), which lasted 100 cycles. This test evaluates the degradation of the catalytic activity of the materials, during cycling. **Figure 9A** shows that before the AST, the highest oxidation- and reduction-peak currents were obtained with SB carbon as a catalyst. However, after the AST, peak areas associated with the charge transferred during oxidation, were depleted by about 70% (**Figure 10**) from their initial value. However, peak currents of SB carbon were still the highest, even after the AST (**Figure 9B**). The lowest depletion of the oxidation peak area among the tested materials of  $\sim 35\%$ , was that of Vulcan XC72R. On the other hand, this material showed a quite high loss of  $\sim 50\%$  of reduction peak area. BP 2000 showed the lowest decrease in reduction-peak area ( $\sim 24\%$ ), and the greatest decrease in oxidation-peak area ( $\sim 90\%$ ).

Oxidation peak area of TiC before AST was already small relatively to other materials, but slightly higher than that of

BP 2000 (see **Table 2**). As we found, the surface of titanium carbide is strongly oxidized. **Figure 11** shows high-resolution XPS spectrum of Ti2p core levels acquired from the surface of TiC powder. The strong  $\text{TiO}_2$  peaks indicate that about 46% of the surface of the powder was mostly consisted of this type of oxide. About 15% of  $\text{TiOC}$  and about 5% of titanium oxides of different stoichiometry could also be observed on the surface. The presence of the oxide layer on TiC explains its low OER activity, as in the case of lithium-oxygen batteries (Adams et al., 2014) and in agreement with Density Functional Theory (DFT) calculations (Landa-Medrano et al., 2018). In Landa-Medrano et al. (2018) it was found that after deposition of two molecular layers of alkali-metal oxides, the initial state of the TiC surface becomes unimportant, and that adsorption energies of  $\text{Na}_2\text{O}_2$  and  $\text{NaO}_2$  approach their native crystal values. Although, in this work the area of reduction peak of TiC was found to be larger than those of BP 2000 and about the same as of Vulcan XC72R catalyst, it is still much smaller than of  $\text{Ni}_x\text{Co}_y\text{O}_z$  powders, indicating lower catalytic activity for OER (see **Table 2**).

Despite the expectation that the catalytic activity of TiC deteriorates not as much as of carbon, after 100 cycles, it showed the greatest loss of reduction peak area ( $\sim 57\%$ ) (**Figure 10**). It also exhibited higher loss of oxidation peak area than Vulcan XC72R ( $\sim 68\%$  vs.  $\sim 35\%$ ), but lower than BP 2000 ( $\sim 90\%$ ) and SB carbon ( $\sim 72\%$ ). The reason for such a high OER and ORR degradation probably comes from some still non-identified surface changes of the powder during the AST. The highest change of the double layer capacity normalized to BET, among the tested materials clearly points out strong surface changes or loss of adhesion of the catalyst powder to the GC electrode during the AST (**Figure 12**).

From **Figure 10** we can see that in general, the examined materials, exhibited more significant depletion of the oxidation than the reduction peak areas after 100 consecutive cycles. While the degradation of the charge transferred during the oxidation



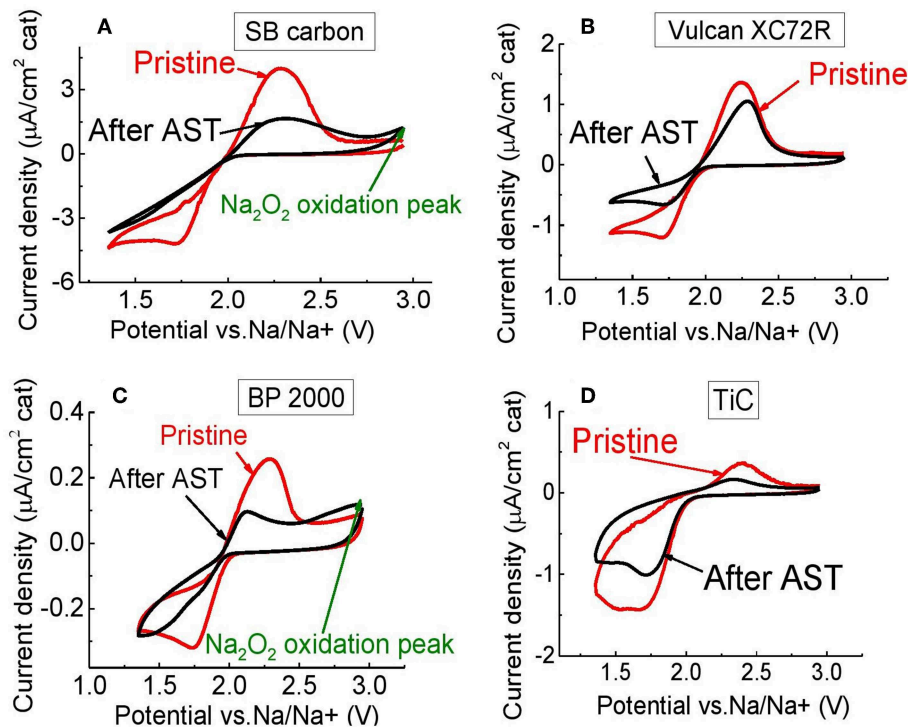


**FIGURE 13** | Electrochemical performance of (A) SB carbon, (B) Vulcan XC72R, (C) BP 2000, (D) TiC, before and after durability test, in PEGDME/0.25 M NaOTf (Scan rate 5 mV/s).

process after a durability test for the Vulcan XC72R catalyst was somewhat lower than during reduction (Figure 10), we suggest that in most cases it is the OER process, which exhibits stronger deterioration. In order to explain this phenomenon, additional examination of surface of the materials before and after the AST should be conducted, which is in progress.

After the AST, the ORR peaks on BP 2000 (Figure 13C) and SB carbon electrodes (Figure 13A) were shifted from 1.73 to 1.31 V and from 1.71 to 1.36 V, respectively. This shift could be caused by blockage of the electrode surface with discharge products, during cycling. SB carbon exhibited the highest change in double-layer capacity (~38%) among the tested carbons, which supports the assumption of clogging of the surface area of the electrode. However, BP 2000 showed very little (about 4%) change in the double-layer capacity (Figure 12). Therefore, we speculate that for BP 2000 this shift can be attributed to electrochemical formation of  $\text{Na}_2\text{O}_2$  (Equation 3). For Vulcan XC72R and for TiC the shift was not observed (Figures 13B,D), presumably as a result of more effective oxidation of the reduction products during cycling, and therefore less clogging of the electrode surface. However, the double-layer capacity of Vulcan XC72R changed by about 15%, which indicates that its surface was slightly changed during AST.



In addition, the appearance of the second oxidation peak, which is probably attributed to  $\text{Na}_2\text{O}_2$  oxidation,

could be clearly distinguished in the CVs of BP 2000 and SB carbons (Figures 13A,C) after the AST. This  $\text{Na}_2\text{O}_2$  compound could be generated either electrochemically or via chemical disproportionation of  $\text{NaO}_2$ . For Vulcan XC72R this peak was not observed in the selected electrochemical window, probably indicating the formation of a much smaller amount of  $\text{Na}_2\text{O}_2$ .

## CONCLUSIONS

The significance of the use of high-surface-area materials for the accommodation of low-conductivity discharge products was presented. It was shown that on cycling, the peak current decreases to a much lesser degree on the electrode coated with Black pearls 2000, than on the neat GC.

Different crystal phases were detected in synthesized  $\text{Ni}_x\text{Co}_y\text{O}_z$  powders with different relative nickel and cobalt content, and annealing temperatures. The highest activity was obtained with the use of a powder, which contained 45%  $\text{NiCo}_2\text{O}_4$ , 10% CoO, 30% metallic nickel, and 15% metallic cobalt. We believe that the metallic nickel and cobalt phases are responsible for this high catalytic activity. However, additional studies should be conducted in order to evaluate quantitative contribution of these metallic phases to the catalytic properties of the powders. All the

synthesized  $Ni_xCo_yO_z$  powders showed better activity than BP 2000. Molecular dynamic simulation studies of adsorption energies of oxygen and  $NaO_2$  molecules on the surface of the catalyst components could be helpful for the explanation of the findings mentioned above. Such work is planned to be done.

Accelerated stress tests of 100 CV cycles, which were carried out for TiC, BP 2000, SB carbon and Vulcan XC72R powders, revealed that TiC exhibited the greatest loss of reduction peak area ( $\sim 57\%$ ) during the test, indicating the highest loss of catalytic activity. It also exhibited higher loss of oxidation peak area than Vulcan XC72R ( $\sim 68\%$  vs.  $\sim 35\%$ ), but lower than BP 2000 ( $\sim 90\%$ ) and SB carbon ( $\sim 72\%$ ). The reason for such a high degradation probably comes from strong surface changes or loss of adhesion of the catalyst powder to the GC electrode during the AST. It was suggested that in most cases, it is the OER process, which exhibits stronger deterioration.

## REFERENCES

- Adams, B. D., Black, R., Radtke, C., Williams, Z., Mehdi, B. L., Browning, N. D., et al. (2014). The importance of nanometric passivating films on cathodes for Li-air batteries. *ACS Nano* 8, 12483–12493. doi: 10.1021/nn505337p
- Bender, C. L., Bartuli, W., Schwab, M. G., Adelhelm, P., and Janek, J. (2015). Toward better sodium-oxygen batteries: a study on the performance of engineered oxygen electrodes based on carbon nanotubes. *Energy Technol.* 3, 242–248. doi: 10.1002/ente.201402208
- Bender, C. L., Hartmann, P., Vračar, M., Adelhelm, P., and Janek, J. (2014). On the thermodynamics, the role of the carbon cathode, and the cycle life of the Sodium Superoxide ( $NaO_2$ ) battery. *Adv. Energy Mater.* 4:1301863. doi: 10.1002/aenm.201301863
- Elia, G. A., Hasa, I., and Hassoun, J. (2016). Characterization of a reversible, low-polarization sodium-oxygen battery. *Electrochim. Acta* 191, 516–520. doi: 10.1016/j.electacta.2016.01.062
- Hartmann, P., Bender, C. L., Vračar, M., Dürr, A. K., Garsuch, A., Janek, J., et al. (2013). A rechargeable room-temperature sodium superoxide ( $NaO_2$ ) battery. *Nat. Mater.* 12, 228–232. doi: 10.1038/nmat3486
- Hartmann, P., Grübl, D., Sommer, H., Janek, J., Bessler, W. G., and Adelhelm, P. (2014). Pressure dynamics in metal-oxygen (metal-air) batteries: a case study on sodium superoxide cells. *J. Phys. Chem. C* 118, 1461–1471. doi: 10.1021/jp4099478
- Kim, J., Park, H., Lee, B., Seong, W. M., Lim, H.-D., Bae, Y., et al. (2016). Dissolution and ionization of sodium superoxide in sodium-oxygen batteries. *Nat. Commun.* 7:10670. doi: 10.1038/ncomms10670
- Kwak, W.-J., Chen, Z., Yoon, C. S., Lee, J.-K., Amine, K., and Sun, Y.-K. (2015). Nanoconfinement of low-conductivity products in rechargeable sodium-air batteries. *Nano Energy* 12, 123–130. doi: 10.1016/j.nanoen.2014.11.057
- Landa-Medrano, I., Ruiz de Larramendi, I., and Rojo, T. (2018). Modifying the ORR route by the addition of lithium and potassium salts in  $Na-O_2$  batteries. *Electrochim. Acta* 263, 102–109. doi: 10.1016/j.electacta.2017.12.141
- Laoire, C. O., Mukerjee, S., Abraham, K. M., Plichta, E. J., and Hendrickson, M. A. (2009). Elucidating the mechanism of oxygen reduction for lithium-air battery applications. *J. Phys. Chem. C* 113, 20127–20134. doi: 10.1021/jp908090s
- Li, Y., Yadegari, H., Li, X., Banis, M. N., Li, R., and Sun, X. (2013). Superior catalytic activity of nitrogen-doped graphene cathodes for high energy capacity sodium-air batteries. *Chem. Commun.* 49, 11731–11733. doi: 10.1039/c3cc46606j
- Liu, T., Kim, G., Casford, M. T. L., and Grey, C. P. (2016). Mechanistic insights into the challenges of cycling a nonaqueous  $Na-O_2$  battery. *J. Phys. Chem. Lett.* 7, 4841–4846. doi: 10.1021/acs.jpclett.6b02267
- Liu, W., Sun, Q., Yang, Y., Xie, J.-Y., and Fu, Z.-W. (2013). An enhanced electrochemical performance of a sodium-air battery with graphene nanosheets as air electrode catalysts. *Chem. Commun.* 49, 1951–1953. doi: 10.1039/c3cc00085k
- Liu, W.-M., Yin, W.-W., Ding, F., Sang, L., and Fu, Z.-W. (2014).  $NiCo_2O_4$  nanosheets supported on Ni foam for rechargeable nonaqueous sodium-air batteries. *Electrochem. Commun.* 45, 87–90. doi: 10.1016/j.elecom.2014.05.021
- Ma, J.-L., Meng, F.-L., Xu, D., and Zhang, X.-B. (2017). Co-embedded N-doped carbon fibers as highly efficient and binder-free cathode for  $Na-O_2$  batteries. *Energy Storage Mater.* 6, 1–8. doi: 10.1016/j.ensm.2016.09.002
- Ottakam Thotiyil, M. M., Freunberger, S. A., Peng, Z., Chen, Y., Liu, Z., and Bruce, P. G. (2013). A stable cathode for the aprotic  $Li-O_2$  battery. *Nat. Mater.* 12:1050. doi: 10.1038/nmat3737
- Peled, E., Golodnitsky, D., Mazor, H., Goor, M., and Avshalomov, S. (2011). Parameter analysis of a practical lithium- and sodium-air electric vehicle battery. *J. Power Sources* 196, 6835–6840. doi: 10.1016/j.jpowsour.2010.09.104
- Pinedo, R., Weber, D. A., Bergner, B., Schröder, D., Adelhelm, P., and Janek, J. (2016). Insights into the chemical nature and formation mechanisms of discharge products in  $Na-O_2$  batteries by means of operando X-ray diffraction. *J. Phys. Chem. C* 120, 8472–8481. doi: 10.1021/acs.jpcc.6b00903
- Raz, K., Tereshchuk, P., Golodnitsky, D., and Natan, A. (2018). Adsorption of  $Li_2O_2$ ,  $Na_2O_2$ , and  $NaO_2$  on  $TiC(111)$  Surface for metal-air rechargeable batteries: a theoretical study. *J. Phys. Chem. C* 122, 16473–16480. doi: 10.1021/acs.jpcc.8b01983
- Schröder, D., Bender, C. L., Osenberg, M., Hilger, A., Manke, I., and Janek, J. (2016). Visualizing current-dependent morphology and distribution of discharge products in sodium-oxygen battery cathodes. *Sci. Rep.* 6:24288. doi: 10.1038/srep24288
- Shang, M., Liu, Y., Xia, J., Zhang, S., and Yang, J. (2017). Synthesis and characterization of  $MnCo_2O_4$  microspheres based air electrode for rechargeable sodium-air batteries. *Ceram. Int.* 43, 3218–3223. doi: 10.1016/j.ceramint.2016.11.147
- Sun, Q., Yadegari, H., Banis, M. N., Liu, J., Xiao, B., Wang, B., et al. (2015). Self-stacked nitrogen-doped carbon nanotubes as long-life air electrode for sodium-air batteries: elucidating the evolution of discharge

## DATA AVAILABILITY STATEMENT

The datasets generated for this study are available on request to the corresponding author.

## AUTHOR CONTRIBUTIONS

EP and DG: conceptualization. EF-S: writing—original draft preparation. DG and EP: writing—review and editing. EF-S: investigation. EP, DG, and AN: supervision.

## FUNDING

The authors would like to thank the Israeli Committee for Higher Education, the Israeli Prime Minister's Office via the INREP project under grant number 07250442001 and the I-SAEF Foundation under grant number PA1359959 for continued support of the project.

- product morphology. *Nano Energy* 12, 698–708. doi: 10.1016/j.nanoen.2015.01.018
- Tseung, A. C. C., and Jasem, S. (1977). Oxygen evolution on semiconducting oxides. *Electrochim. Acta* 22, 31–34. doi: 10.1016/0013-4686(77)85049-4
- Yadegari, H., Banis, M. N., Xiao, B., Sun, Q., Li, X., Lushington, A., et al. (2015). Three-dimensional nanostructured air electrode for sodium–oxygen batteries: a mechanism study toward the cyclability of the cell. *Chem. Mater.* 27, 3040–3047. doi: 10.1021/acs.chemmater.5b00435
- Yadegari, H., Li, Y., Norouzi Banis, M., Li, X., Wang, B., Sun, Q., et al. (2014). On rechargeability and reaction kinetics of sodium–air batteries. *Energy Environ. Sci.* 7, 3747–3757. doi: 10.1039/C4EE01654H

**Conflict of Interest:** The authors declare that the research was conducted in the absence of any commercial or financial relationships that could be construed as a potential conflict of interest.

Copyright © 2019 Faktorovich-Simon, Natan, Peled and Golodnitsky. This is an open-access article distributed under the terms of the Creative Commons Attribution License (CC BY). The use, distribution or reproduction in other forums is permitted, provided the original author(s) and the copyright owner(s) are credited and that the original publication in this journal is cited, in accordance with accepted academic practice. No use, distribution or reproduction is permitted which does not comply with these terms.